Review (Invited)

Microscopic Analysis of Graphene and Carbon Nanotube Growth

Yoshikazu Homma *
Department of Physics, Tokyo University of Science, Shinjuku, Tokyo 162-8601, Japan
* *homma@rs.tus.as.jp*

（Received: July 15, 2017; Accepted: October 24, 2017）

We have observed chemical vapor deposition (CVD) processes of single-walled carbon nanotubes (SWCNTs) using scanning electron microscopy (SEM) by repeating ethanol exposure and observation without ethanol at an elevated temperature. The initial stage of SWCNT growth and their extension process were analyzed on the SiO_2/Si substrate. On the patterned substrate, suspended SWCNT formation processes were successfully traced. Both the observations of growth on the substrate and that between mesa patterns suggest fluctuation of SWCNT growth direction during CVD cause SWCNTs falling on the substrate, forming nearest neighbor suspension and bundling. For graphene segregation on the nickel surface, the formation process could be observed by SEM, enabling preparation of layer-number defined graphene specimens useful for the researches of secondary electron image formation.

1. Introduction

In situ microscopy of crystal growth provides insight into the growth mechanism, and it has successfully been applied to growth in ultrahigh vacuum or molecular beam epitaxy environment. For nanocarbon materials, single walled-carbon nanotube (SWCNT) and graphene, however, chemical vapor deposition (CVD) at higher-pressure gas environment is used for growth. An observation method capable in a gas environment at high temperatures is necessary for nanocarbon materials. We have employed scanning electron microscopy (SEM) for the observation of monolayer growth and sublimation on various material surfaces [1]. SEM is advantageous in the wide field of view ranging up to millimeter, and capability of gas introduction in the observation chamber. For SWCNTs, the formation process of suspended SWCNTs between micro-pillars [2] and the extension process of SWCNTs on SiO_2 substrates [3, 4] were observed by repeating CVD and SEM observation alternately in the SEM chamber. For graphene, monolayer segregation processes [5] as well as nucleation processes [6] were observed on polycrystalline Ni surfaces by SEM. Recently, in situ SEM was applied to CVD growth of graphene on polycrystalline Cu [7].

In this review, in situ observations of SWCNTs are introduced and growth processes of SWCNTs are discussed. For graphene, segregation processes on a nickel substrate are shown and the image formation mechanism is discussed.

2. Methods

The SEM instrument used for in situ observations was LEO 1530VP (Carl Zeiss), which could be operated at a low vacuum condition (1-100 Pa). The LEO 1530 VP has two types of SE detector: One is so-called in-column detector set in the Gemini column [8], and the other is a normal Everhart-Thornley detector [9] (so-called out-lens detector). The in-column detector was mainly used in this study. The out-lens detector was supplementally used for graphene observation (in section 3.2). We have added a gas inlet system to the SEM specimen chamber [2]. SWCNT-CVD was performed by exposing the specimen to ethanol vapor at 770-780°C. Heating of SiO_2/Si specimens was done by passing through a direct current to the silicon substrate. The temperature of the specimen was measured with an infrared optical pyrometer through a sapphire view port. Normal SEM observation was performed at 1×10^{-4} Pa. For the growth ex-

periment, ethanol vapor of 27 Pa was introduced into the specimen chamber with the flow rate of 30 sccm. During CVD growth, the electron beam was not directed to the specimen surface avoiding any damage of nanotubes caused by electron-beam irradiation. The gas environment hindered the detection of secondary electrons in a normal way. Although environmental SEM could acquire images in the gas ambience by collecting avalanche electrons, the image contrast was not high enough to obtain individual SWCNT images. Thus, the chamber was pumped to 1×10^{-4} Pa for SEM observation. For the observation of the growth process successively, ethanol exposure and observation without ethanol were repeated with keeping the substrate temperature at 780ºC. The acceleration voltage of the primary electron beam was 0.5-1 kV. All the images were taken at normal incidence of the electron beam.

Graphene was synthesized by segregation on the Ni surface at the elevated temperatures, which could be monitored by SEM in real time. The Ni specimen used was a 0.1 mm-thick Ni (> 99 %) foil whose surface was mechanically polished. The foil was cut into a 0.3 mm × 2 mm sized piece so as to be heated to ~1000°C with a dc current of ~5 A in the SEM chamber. Before the in-situ SEM observations, the specimen was annealed at 950°C in an Ar/H_2 (3% H_2 by volume) mixture gas for enlargement of Ni grains in a quartz furnace. Then, a carbon film (in the form of small-sized grains of graphite) was deposited using ethanol vapor supplied by bubbling liquid ethanol with an Ar/H_2 gas (total pressure of 800 Pa) at 900°C for 20 min. During in situ observations, we estimated the specimen temperature based on the behavior of graphene either dissolving (>900°C) or monolayer and multilayer segregation (~790–900°C).

3. SWCNT Growth

3.1 Growth processes on substrate

The initial stage of SWCNT growth on the SiO_2 (100 nm-thick)/Si substrate is depicted in Fig. 1, by repeating a short-time growth and observation [3]. SEM images observed at the cumulative growth of 20, 40, 220, and 1000 s are shown in Fig. 1. In the very initial stage, bright spots appeared on the surface (Fig. 1a). They are short SWCNTs standing (not lying down) on the substrate. Then the image turned quite different as shown in Fig. 1c. Bright spots decreased and moss-like patterns

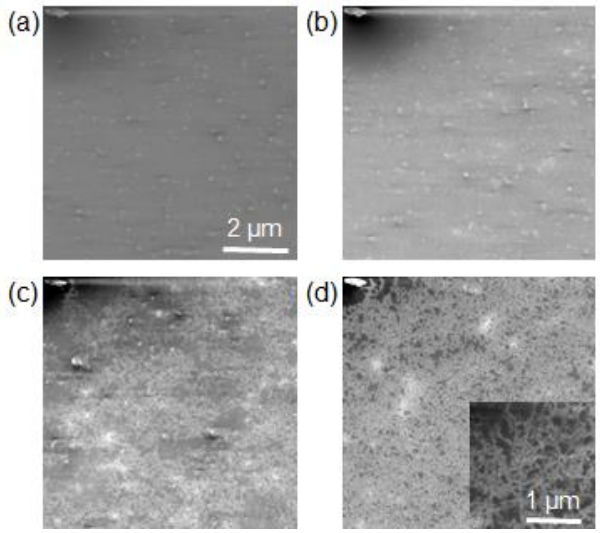

Fig. 1. Sequential observation of initial stage of SWCNT growth on SiO_2. Cumulative growth time: (a) 20 s, (b) 40 s, (c) 220 s, and (d) 1000 s. Inset in (d) is a magnified SEM image.

appeared. Finally, the moss-like patterns covered all over the surface (Fig. 1d). The moss-like patterns are caused by SWCNTs lying down on the SiO_2 substrate [10]. A higher magnification image is shown in the inset in Fig. 1d. Thus, in contrast to the very initial stage, SWCNTs lay down on the substrate surface. These results indicate that SWCNTs initially grow in the random direction, then, long SWCNTs fall on the substrate surface. The coverage of SWCNT increased with increasing the growth time.

The question is whether the coverage increase is due to the increase of newly grown nanotubes or extension of existing nanotubes. To investigate this issue, we need sparsely distributed catalysts to observe individual SWCNT growth. Thus, we used Co-filled apoferritin dispersed in ethanol and spin-coated on the SiO_2/Si substrate [11]. After calcinations of Co-filled apoferritin, dispersed Co nanoparticles with diameters 4.7±0.7 nm were obtained. By exposing to the ethanol vapor at 770°C, SWCNTs were grown on SiO_2. Raman spectra of those nanotubes (not shown) exhibited radial breathing modes ranging from 100 to 250 cm^{-1}, indicating presence of SWCNTs with diameters of 1-2 nm. When SEM images were observed at the same place on the SiO_2 surface with a 5 or 10-min-growth duration, some nanotubes showed continuous extension, while most nanotubes remained unchanged.

We found about 16 re-growth cases out of 97

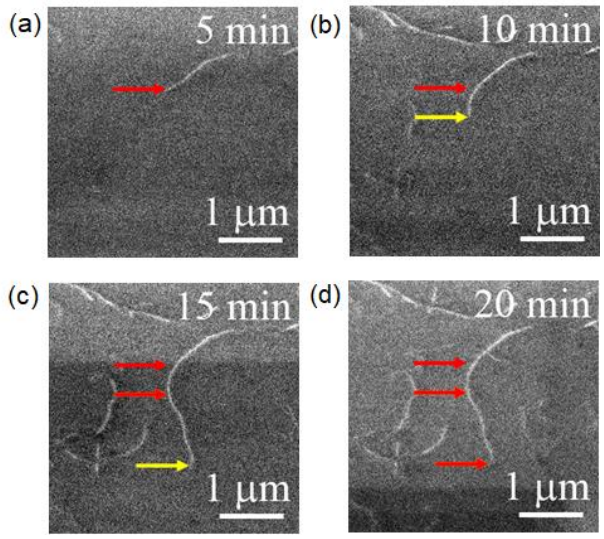

Fig. 2. (color online) Extension process of SWCNT on SiO2 substrate observed with 5-min growth duration. Cumulative growth time: (a) 5 min, (b) 10 min, (c) 15 min, and (d) 20 min. Arrows indicate the growing tip of the SWCNT.

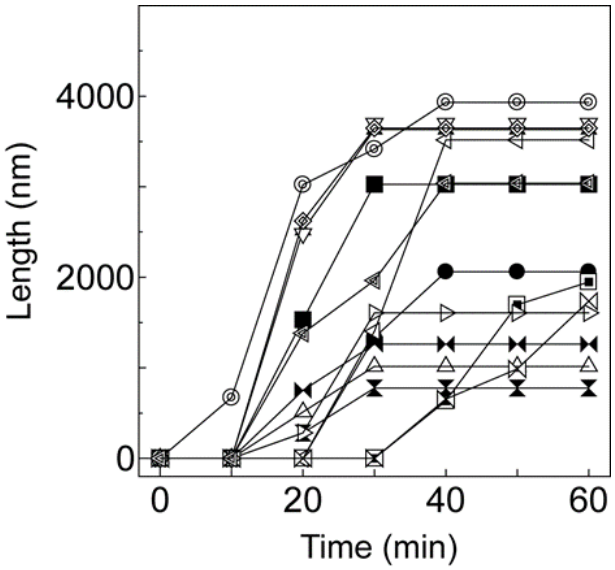

Fig. 3. Time evolution of length for individual SWCNTs [4].

nanotubes. An example of continuous extension is shown in Fig. 2 for total 20-min growth with four times repetition of a 5-min growth duration [4]. After 5 min from starting growth, a 1-μm nanotube was found. After another 5-min growth, the nanotube had extended by 0.5 μm. In the next 5-min growth, it further extended by 1 μm, and never showed further re-growth. Thus, the active growth period was within 15 min. Furthermore, the nanotube shape which had been observed in the previous frame did not change before and after extension.

From such observations, we plotted time evolution of nanotube length in Fig. 3 for the 10-min growth duration [4]. This plot leads to interesting conclusions. (i) Each growth curve showed an incubation time before starting growth, and it ranged from less than 5 min to 30 min. (ii) Total growing duration was limited to about 20 min, and the maximum length was limited to less than 4 μm in most cases. (iii) As a result of these two features, growth rarely occurred after 40 min in 27 Pa. The results confirmed the presence of incubation time for individual nanotubes. The difference of the incubation time for each nanotube is likely relating to the size difference of catalyst particles. Also, the results indicate a finite lifetime of catalyst in the two senses. One is that after the incubation time the active duration of catalyst is limited. The other is that after certain period (30−40 min in the present experimental condition) no growth occurs. The incubation time and the lifetime depended on the ethanol pressure, and they were longer for lower pressures. But, the final length of nanotubes was almost the same irrespective of the pressure.

Most SWCNTs were short, 2 μm in average. They did not show extension on the substrate when observed even with a 5 min interval. We think that short SWCNTs have been produced from catalyst particles with short lifetimes. The lifetime was less than the 5-min growth duration. Those SWCNTs that showed extension were grown from longer-lifetime catalyst particles. The longer-lifetime catalyst particles were 16% of the active catalyst particles. There was no correlation between the incubation time and the lifetime. The factor that differentiates catalyst lifetime is unclear. It is possibly the local chemistry of catalyst particles, such as graphite shell formation around the catalyst.

3.2 Growth processes on patterned substrate

SWCNT grown from a mesa pattern to the space is free from the interaction with the substrate. Thus, it is interesting to observe extension process. Moreover, this kind of observation can elucidate the formation process of suspended SWCNTs between pillar patterns [11].

Successive SEM images observed every 10 min during CVD using SiO_2 mesa patterns are shown in Fig. 4. The pattern was a square lattice of 300 nm×300 nm SiO_2 pillars with 300 nm high. A suspended nanotubes indicated by an arrow emerged after 10 min growth from the lower

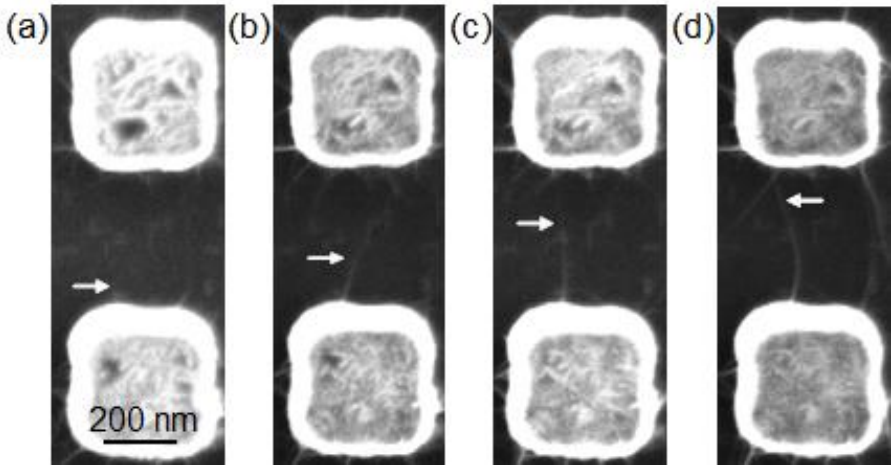

Fig. 4. Sequential observation of suspended SWCNT growth between SiO2 mesa patterns. Cumulative growth time: (a) 10 min, (b) 20 min, (c) 40 min, and (d) 50 min.

pillar (Fig. 4a). It grew longer in Fig. 4b. Interestingly, it changed the direction in Fig. 4c. Finally, it formed a bridge between the lower and upper pillars. Thus, continuous growth takes palace when a SWCNT is free from the substrate.

Another important finding from the observation is that the extension direction of a SWCNT changes during growth. It has been shown that the bridging probability between the first neighbor pillars is much higher than that between the second neighbor pillars arranged in a square lattice [12, 13]. The fluctuation of the extension direction of growing SWCNT explains the preference of nearest neighbor bridge formation. This also explains why SWCNTs tend to form bundles. Due to lively movement of SWCNTs during growth, they may touch each other and form bundles.

4. Graphene Imaging

Graphene is a monolayer material composed of carbon honeycomb lattice. When carbon doped Ni is slowly cooled from above 900˚C, carbon atoms segregate to the surface of Ni and form monolayer graphene [14]. Above 900°C, carbon atoms are dissolved in the Ni bulk. At around 900−790°C, monolayer graphene segregates and further segregation to form multilayer graphene occurs below 790°C. The segregation temperature, though, depends on the carbon concentration in Ni [15]. For lower carbon concentrations, the temperature range of monolayer graphene segregation shifts to lower temperature by ≈100°C.

The effect of graphene on SE emission is not large except for the insulator surface where charging is compensated by the graphene overlayer [16]. There are several image formation mechanisms. On an insulator surface, charging state difference causes the SE contrast; darker on the positively charged insulator surface and brighter on the monolayer-graphene covered surface. On an air-exposed metal surface, the difference between oxidized and non-oxidized surfaces is responsible for the SE contrast; generally brighter on the oxidized metal surface and darker on the monolayer-graphene covered (non-oxidized) surface. On a polycrystalline surface, crystal orientation of each grain causes SE contrasts due to electron channeling or work function difference, which makes recognition of few-layer graphene difficult. However, during segregation of graphene on the metal surface, the edge of graphene can be clearly observed by SEM [5]. Above 400˚C, the edge contrast of monolayer graphene becomes prominent, thus, monolayer graphene can be distinguished from Ni grains in SE images.

The SE contrast of graphene depends on the type of detector used; the in-column detector and the out-lens detector. Figure 5 shows in-situ SE images of graphene growing on a large Ni (111) grain surface during heating at ≈800°C. SE images simultaneously acquired with the in-column and out-lens detectors are shown in the left and right parts of the SE images, respectively. For monolayer graphene, the SE image acquired with the in-column detector exhibits prominent edge contrast, which accentuates the monolayer graphene on the Ni surface [5, 6]. The edge contrast appears as either bright (for the right edge in Fig. 5) or dark (for the upper and left edges) depending on the inclination of the substrate surface or the non-uniformity of the detection efficiency.

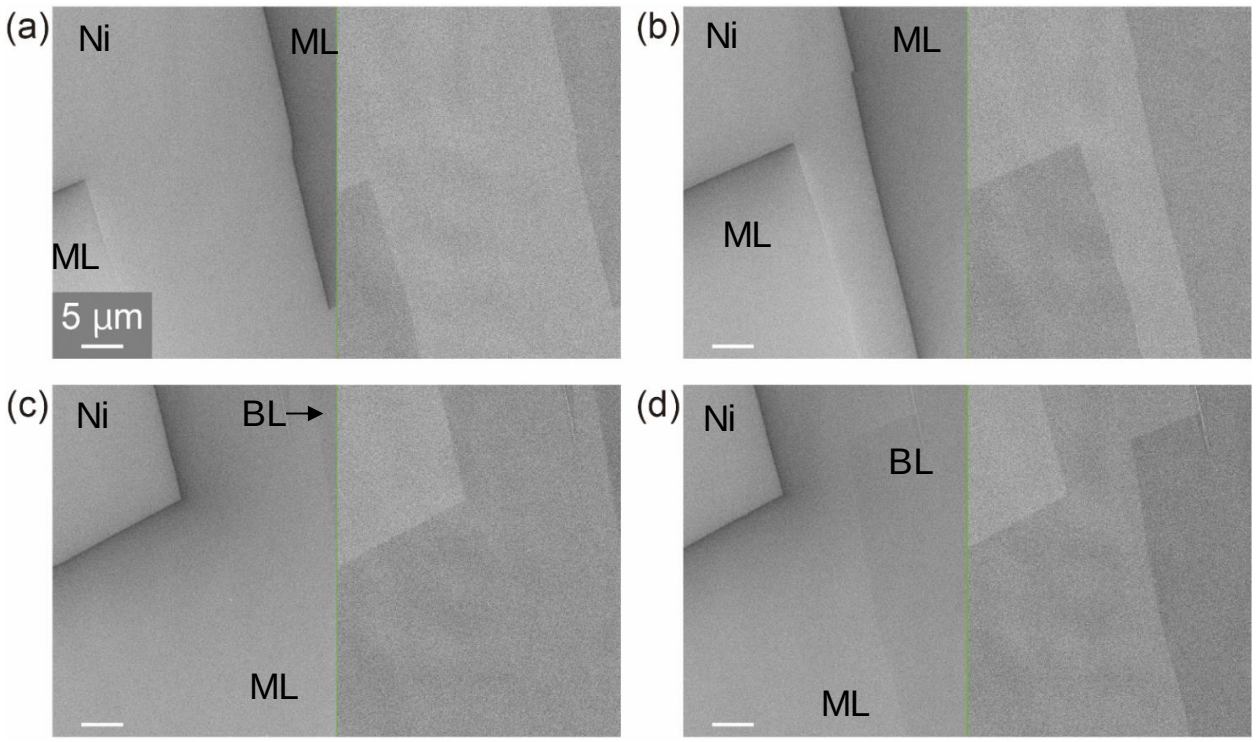

Fig. 5. In situ SE imaging of graphene segregation process on a wide Ni(111) grain surface observed at ~800°C. SE images simultaneously acquired with the in-column (left half) and out-lens (right half) detectors are shown. Images (a)-(d) were acquired every ≈30 s. During observation, two domains of monolayer graphene (ML) proceeded from left and right ends of the view field, and merged at the center in (c). The second layer (BL) appeared in (d).

Apart from the edge contrast, the brightness of graphene covered region is almost the same as the bare Ni surface. In contrast, no such edge contrasts appear in the SE image acquired with the out-lens detector. On the other hand, the graphene covered regions appear clearer as a darker contrast. The further darker area seen in Fig. 5d is the second layer of graphene segregated underneath the first layer. Although the second layer can also be recognized in the SE image acquired with the in-column detector, the contrast is less prominent and the edge contrast is absent. The differences in the SE images of graphene between the two types of detectors should be originated from the difference in the energy range detected. Lower energy SEs are mainly collected with the in-lens detector and the remaining higher energy portion is collected with the out-lens detector. The details of the energy-dependent graphene images will be reported elsewhere [17].

5. Summary

In situ SEM was used to track the growth processes of SWCNTs on the SiO_2 substrate and between mesa structures. Although our observations were not done in real time, we could obtain two important results: initially, SWCNTs grew into random directions on the substrate, but they fell on the substrate surface when grew longer; and the direction of tube axis fluctuated during growth into free space. These two results are consistent with each other. Due to fluctuation during growth, a SWCNT tends to lie down on the surface. This also consistent with strong tendency of bundle formation and the high probability of nearest neighbor bridge formation for suspended SWCNTs. Furthermore, a large spread of incubation time was found when individual SWCNT growth was tracked using sparsely dispersed catalyst particles.

Monolayer graphene can be imaged by SEM, although it is almost transparent to the secondary electrons generated in the underneath material. At elevated temperatures, graphene edges exhibited prominent topographic contrast: either brighter or darker contrast depending on the relationship between the edge direction and the anisotropy in SE detection efficiency. For thicker layers of graphene, the SE intensity decreased with an increase in the number of layers. The differences in the detecting SE energy range affected SE contrasts between few layer graphene.

6. Acknowledgment

The in situ SEM researches were supported by CREST, Japan Science and Technology Agency, a Grant-in-Aid for Scientific Research on Priority Areas (No 19054015) and a Grant-in-Aid for Scientific Research on Innovative Areas (No. 15H05869) from the Ministry of Education, Culture, Sports, Science and Technology (MEXT), Japan.

7. References

[1] Y. Homma, in Handbook of Crystal Growth, 2nd Edn., ed. by T. Nishinaga, Chapt. 14, pp. 1003-1030, Elsevier, Amsterdam (2014).
[2] Y. Homma, D. Takagi, and Y. Kobayashi, *Appl. Phys. Lett.* **88**, 023115 (2006).
[3] D. Takagi, Y. Homma, S. Suzuki, and Y. Kobayashi, *Surf. Interface Anal.* **38**, 1743 (2006).
[4] I. Wako, T. Chokan, D. Takagi, S. Chiashi, and Y. Homma, *Chem. Phys. Lett.* **449**, 309 (2007).
[5] K. Takahashi, K. Yamada, H. Kato, H. Hibino, and Y. Homma, *Surf. Sci.* **606**, 728 (2012).
[6] Y. Momiuchi, K. Yamada, H. Kato, Y. Homma, H. Hibino, G. Odahara and C. Oshima, *J. Phys. D: Appl. Phys.* **47**, 4553011 (2014).
[7] Z.-J. Wang, G. Weinberg, Q. Zhang, T. Lunkenbein, A. Klein-Hoffmann, M. Kurnatowska, M. Plodinec, Q. Li, L. Chi, R. Schloegl, and M.-G. Willinger, *ACS Nano*, **9**, 1506 (2015).
[8] H. Jaksch, J. P. Martin, *Fresenius J. Anal. Chem.* **353**, 378 (1995).
[9] T. E. Everhart and R. F. M. Thornley, *J. Sci. Instrum.* **7**, 246 (1960).
[10] Y. Homma, S. Suzuki, Y. Kobayashi, M. Nagase, and D. Takagi, *Appl. Phys. Lett.* **84**, 1750 (2004).
[11] G.-H. Jeong, A. Yamazaki, S. Suzuki, H. Yoshimura, Y. Kobayashi and Y. Homma, *J. Am. Chem. Soc.* **127**, 8238 (2005).
[12] Y. Homma, Y. Kobayashi, T. Ogino, and T. Yamashita, *Appl. Phys. Lett*. **81**, 2261 (2002).
[13] T. Matsumoto, Y. Homma and Y. Kobayashi, *Jpn. J. Appl. Phys.* **44**, 7709 (2005).
[14] J. C. Shelton, H. R. Patila, and J. M. Blakely, *Surf. Sci.* **43**, 493 (1974).
[15] M. Eizenberg and J. M. Blakely, *Surf. Sci.* **82**, 228 (1979).
[16] H. Hiura, H. Miyazaki, and K. Tsukagoshi, *Appl. Phys. Express*, **3**, 095101 (2010).
[17] K. Shihommatsu, J. Takahashi, Y. Momiuchi, Y. Hoshi, H. Kato, and Y. Homma, *ACS Omega*, **2**, 7831 (2017).

Discussions and Q&A with Reviewers

Reviewer #1 Masaki Tanemura (Nagoya Institute of Technology)

This is a very interesting review, especially on the SWCNT parts.

[Q1_1]

For the easier understanding of readers on the number of layers of graphene, Raman mapping corresponding to Fig. 5 will be helpful (if it is available).

[A1_1]

Actually, the interpretation of Raman data on the Ni surface is not straightforward. Because of the strong interaction between graphene and the Ni surface, monolayer graphene exhibits no G- and 2D-bands that are characteristic Raman peaks of graphene. Bilayer graphene exhibits G- and 2D-bands in the same manner as monolayer graphene. Such the Raman spectra can be found in our previous publication, Ref. 5.

Reviewer #2 Satoshi Hashimoto (JFE Techno-Research)

This manuscript is concerned the growth of CNT and graphene using the in-situ SEM observation. The manuscript is important and helpful for the readers who have interests in the growth of CNT and graphene, and in image contrast in ULV-SEM. It shall be published in this journal.

However, there are some points that it is difficult to follow the author's idea, so some minor revisions are proposed.

[Q2_1] "Method" of chapter 2

It is recommended to add brief explanation for the sample which is written as "disordered graphite"

I am not familiar to the term of this field. However, in the field of the alloys, "disorder" is defined as a crystalline material in which the atomic arrangement is ordered and the occupancy of the lattice is random. Namely, the symmetry is reduced by disordering, but it is crystalline. Considering the crystal structure of the graphite, such disorder may not occur and the "disorder" may mean the amorphous.

[A2_1]

"Disordered graphite" was intended to mean graphite with small-sized grains. Because the Raman spectrum of the film exhibited a large D-band as well as G-band, the film was not amorphous but had graphitic structures. I have changed the term to "small-sized grains of graphite".

[Q2_2] "SWCNT Growth" of chapter 3

Can you add the short explanation about "standing"?

The author writes as "the bright spot in fig.1 (a) are short standing SWCNT". I cannot understand whether it is standing or not.

[A2_2]

SWCNTs lying on the SiO_2 substrate exhibit a peculiar SE contrast like "moss-like patterns" when observed with a low voltage beam as reported in Ref. 10. The bright spot image means that the SWCNTs are not contacting the SiO_2 substrate. To make this point clearer, I have changed the sentence to "They are short SWCNTs standing (not lying down) on the substrate."

[Q2_3]

I cannot understand that the "shape of the existing part of the nanotube" means a point of the substrate that the nanotube growth or the total shape of nanotube itself. So, can you add brief explanation?

The SEM image is easy to understand the structure, but it is sometimes difficult for the people who are not familiar to the specified material to find the parts on which the presenter focuses, because many different structures are seen.

[A2_3]

Here, extension of a nanotube seen in Fig. 2 is discussed. The existing part of the nanotube means that observed in the previous frame. I have changed the sentence to "the nanotube shape which had been observed in the previous frame did not change before and after extension."

[Q2_4] "Graphene Imaging"

Can you comment on the difference between the con-

trast by the in column SE image and the out-lens SE image in Fig.5. Namely, why the edge contrast is seen in the in column SE is seen, but is not seen in the out lens SE.

I think that the out-lens SE image mainly show the surface roughness, and the chemical information is enhanced in the in column SE image. However, the image of Fig. 5 is quite different from such empirical knowledge.

[A2_4]

The contrast is really quite different from the normal topographic contrast. The image difference between the in-column detector and the out-lens detector might be affected by the difference in acceptance range of the take-off angle as well as the energy range of SEs (see Dr. Masayasu Nagoshi's work in these proceedings). Since the topic is still under investigation, I have not commented on it in the revised manuscript.

[Q2_5]

The contrast in Fig.5 is very interesting. The author write as the detail will be reported elsewhere. Can you show the reference?

Especially, the following contrast is interesting.

- The edge contrast seen in in-column SEM image is not seen in out-lens observation
- The edge contrast between Ni surface and mono-layer grapheme is seen, but the edge contrast between second layer and mono-layer is not seen.
- The contrast in mono-layer is same as the substrate in ln-column image, but the contrast of grapheme layer is dark in the out-lens image.

Figure caption of Fig5: The explanation of each photo in 4 photos (a-d) is missing. The explanation is required in the caption.

[A2_5]

Our paper on the energy dependence of graphene layer contrast has just been published, which is added as Ref. 17. The differences in the SE images of graphene between the two types of detectors stem from the difference in the energy ranges detected. However, the cause of the peculiar edge contrast of monolayer graphene remains unclear. Since the edge contrast is created by lower-energy SEs, it appears only in the images acquired with the in-column detector. Also, the large acceptance range of take-off angle of the in-column detector might be responsible to the clear edge contrast.

I have added the explanation that the images (a)-(d) were acquired every 30 s during heating at ≈800°C in the figure caption of Fig. 5.